

Secondary emission and acoustic-phonon scattering induced by strong magnetic fields in multiple quantum wells

V. F. Sapega,* V. I. Belitsky,* T. Ruf, H. D. Fuchs, M. Cardona, and K. Ploog

Max-Planck-Institut für Festkörperforschung, Heisenbergstrasse 1, D-7000 Stuttgart 80, Federal Republic of Germany

(Received 8 May 1992; revised manuscript received 22 July 1992)

A strong increase of low-frequency Raman scattering has been observed in GaAs/Al_xGa_{1-x}As multiple quantum wells in magnetic fields up to 14 T. The spectra, consisting of background scattering, folded acoustic phonons, and additional features, show resonant behavior with respect to the laser frequency and the strength of the magnetic field. The broad background, usually related to geminate recombination, has its origin in a continuum of Raman processes with the emission of longitudinal-acoustic phonons where crystal momentum is not conserved. Such processes can become dominant when interface fluctuations allow for resonant scattering in individual quantum wells only. Thus phonons with all possible energies contribute to the background scattering efficiency. The observed folded longitudinal-acoustic phonons are in good agreement with calculated frequencies. Additional features, detected in all samples measured, are attributed to local vibrational modes tied to the gaps at the folded Brillouin-zone center and edge. Other peculiarities observed correspond to modes localized at crossings of the folded longitudinal- and transverse-acoustic branches inside the Brillouin zone. The appearance of these local modes is attributed to fluctuations in the well and barrier thicknesses of the quantum wells.

I. INTRODUCTION

The effect of a magnetic field on the intensity of Raman scattering by longitudinal-optic (LO) phonons in bulk semiconductors was studied intensively in recent years.¹⁻³ Theoretical models with various degrees of approximations with respect to the electronic structure and electron-phonon interaction have been reported.⁴⁻⁶ An enhancement of the LO-phonon Raman efficiency in multiple quantum wells (MQW's) and superlattices in a magnetic field was observed in Refs. 7-9. Theoretical treatments of magneto-Raman scattering in quantum wells for the cases of deformation-potential¹⁰ and Fröhlich electron-phonon interaction¹¹ have been published. In investigations of inelastic light scattering at lower energies strong secondary emission near the excitation line was found.¹²

In this paper we report on the investigation of low-frequency Raman spectra in a magnetic field in GaAs/Al_xGa_{1-x}As multiple quantum wells. The magneto-resonant behavior of the oscillatory emission background is studied. Resonances of incoming and outgoing character are found. A theoretical model to explain the origin of this emission based on single-quantum-well effects is developed. In Faraday geometry, i.e., with the wave vector of the light parallel to the field, a rather pronounced increase of the Raman efficiency for scattering by folded longitudinal-acoustic (LA) phonons is found. We also observe the magnetic-field-induced appearance of peculiarities in the spectra at energies where the folded LA dispersion has gaps. These features are suggested to arise from modes which are localized inside the gaps of a one-dimensional linear chain. Similar modes are also found at points inside the Brillouin zone where the LA and transverse-acoustic (TA) phonon dispersions cross.

The latter features are particularly interesting since the LA and TA phonons are expected to be completely decoupled for the (001) surfaces on which our experiments were performed and thus there should be no anticrossings of the LA and TA branches for **k** exactly parallel to [001] in perfect MQW structures.

II. EXPERIMENT

The samples investigated were grown by molecular-beam epitaxy (MBE) on (001) oriented undoped semi-insulating GaAs substrates kept at 580 °C. The MQW's were separated from the wafer substrate by epitaxially grown buffer layers of 0.2- μ m GaAs and 0.5- μ m Al_xGa_{1-x}As. All samples investigated had a 21-Å cap layer, much too thin to have an influence on the vibrational properties and resonance effects presented in this study. The growth rates were 1.0 monolayer/s for GaAs and 1.5 monolayer/s for Al_xGa_{1-x}As. We denote the samples by (well/barrier, *x*, *p*), giving the well and barrier widths in Å. (*x*) is the Al content of the barrier material. (*p*) indicates the number of periods and was chosen so large that effects from the buffer layers on the phenomena investigated can be neglected.

The experiments were carried out in magnetic fields up to 14 T in backscattering Faraday geometry, where the propagation of incident and scattered light was normal to the (001) plane of the sample and parallel to the magnetic field. All spectra were taken using circularly polarized light. We describe the polarization configuration in the notation $\bar{z}(\sigma^\eta, \sigma^\lambda)z$, where \bar{z} and z are the directions of propagation of the exciting and scattered light, respectively. $(\sigma^\eta, \sigma^\lambda)$ with $\eta, \lambda = \pm$ denotes the circular polarization of the exciting σ^η and scattered σ^λ light.

The sign of λ or η corresponds to the sign of the projection of the photon angular momentum on the propagation direction of the exciting light taken as a fixed axis. Magneto-oscillation profiles were measured by choosing an exciting laser energy and setting the spectrometer, a Spex 1404 double monochromator, as a spectral band-pass to the Raman shift of interest. The intensity of scattered light versus magnetic field was then recorded using conventional photon counting techniques.

III. EXPERIMENTAL RESULTS

In magnetic fields stronger than 1 – 2 T we observe the appearance of secondary emission in both Stokes and anti-Stokes regions near the laser excitation line. Spectra of this secondary emission in the Stokes and anti-Stokes regions for sample (98/102, $x=0.34$, $p=40$) are presented in Fig. 1 for magnetic fields of 0 and 11 T in the $\bar{z}(\sigma^+, \sigma^+)z$ scattering configuration. The 11-T spectrum is composed of the secondary-emission background, two doublets LA₁ and LA₂ corresponding to the folded acoustic modes, plus some features marked as LM (local mode). The intensities of these spectra at all “Raman shifts” depend linearly on the power of the exciting laser in the range of 0.1 – 10 W/cm². All points in the spectra, not only those related to folded acoustic-phonon Raman scattering, exhibit pronounced resonances in a magnetic field. Magneto-oscillation spectra of the sample (98/102, $x = 0.34$, $p = 40$) at the point with a Raman shift of 4 cm⁻¹ (not a sharp feature in Fig. 1) are presented in Fig. 2(a) for two polarization configurations $\bar{z}(\sigma^-, \sigma^-)z$ and $\bar{z}(\sigma^+, \sigma^+)z$. In the scattering configurations with crossed polarizations $\bar{z}(\sigma^\pm, \sigma^\mp)z$ the folded acoustic phonons are absent and the intensity of the background is about 100 times smaller. This indicates that both features may have the same origin. The maxima of these oscillations (labeled $n = 1$ to 5)

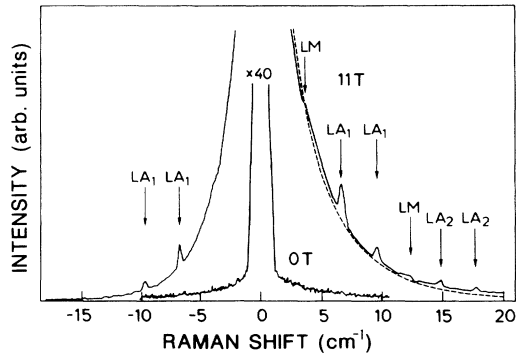


FIG. 1. Raman spectra in the Stokes and anti-Stokes regions for $\bar{z}(\sigma^+, \sigma^+)z$ configuration in magnetic fields of $B = 11$ and 0 T at $T = 6$ K for sample (98/102, $x = 0.34$, $p = 40$). The excitation energy is $\hbar\omega_{\text{ex}} = 1.585$ eV. LA₁ and LA₂ label Raman lines of two doublets of folded acoustic phonons. LM denotes local modes of the BZ edge gap (note the Fano line shape). The dashed line represents the calculated spectrum of light scattered by acoustic phonons for a single QW.

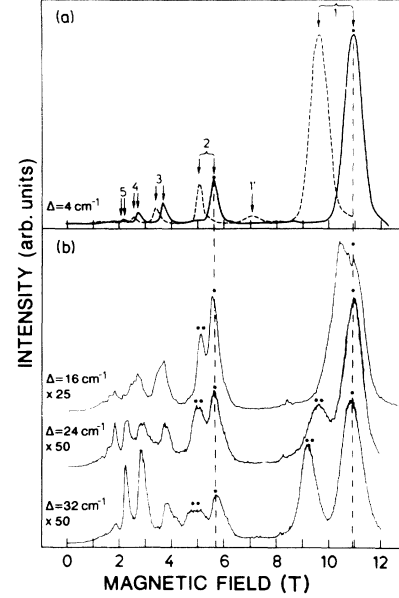


FIG. 2. (a) Intensity oscillations of the background for two polarization configurations $\bar{z}(\sigma^+, \sigma^+)z$ (solid line) and $\bar{z}(\sigma^-, \sigma^-)z$ (dashed line) at a Raman shift of $\Delta = 4$ cm⁻¹ vs magnetic field [$T = 6$ K, $\hbar\omega_{\text{ex}} = 1.588$ eV, sample (98/102, $x = 0.34$, $p = 40$)]. $n = 1 - 5$ labels the transitions between heavy mass and electron Landau levels, $n' = 1$ denotes a light mass to electron inter-Landau-level transition. (b) Intensity of the background for three Raman shifts of $\Delta = 16$, 24, and 32 cm⁻¹ vs magnetic field. The asterisks (*) and (**) mark incoming and outgoing resonances for inter-Landau-level transitions with $n = 1$ and 2, respectively.

can be attributed to resonances of the excitation energy with interband magneto-optical transitions between valence subband Landau states of heavy mass character and conduction electron states. The splitting Δ of the resonances observed in the two scattering configurations of Fig. 2(a) is due to Zeeman splitting of hole and electron Landau levels. For the state $n = 1$ it depends linearly on the field (B); $\Delta/B = (g_e + g_h)\mu_B = 0.3$ meV/T. This yields $g_e + g_h = 5.2$, which is dominated by the heavy-hole g factor, since we estimated the electron g factor to be $g_e = -0.23$ from spin-flip Raman experiments.¹³ The Zeeman splitting of the other Landau levels was found to depend on the excitation energy. In Fig. 2(b) we present magneto-Raman profiles for the $\bar{z}(\sigma^+, \sigma^+)z$ configuration with fixed excitation energy at larger Raman shifts of 16, 24, and 32 cm⁻¹, which again do not correspond to sharp features in the Raman spectra of Fig. 1. In these profiles of the background intensity, resonances with Landau levels of incoming (*) and outgoing (**) character can be distinguished from the observed splitting of the lines. One can see that incoming and outgoing resonances are unresolvable at Raman shifts of less than 16 cm⁻¹ (2 meV). This is due to the inhomogeneous broadening of the magnetoprofiles, caused by a distribution in Landau-level energies originating from well-width fluctuations.

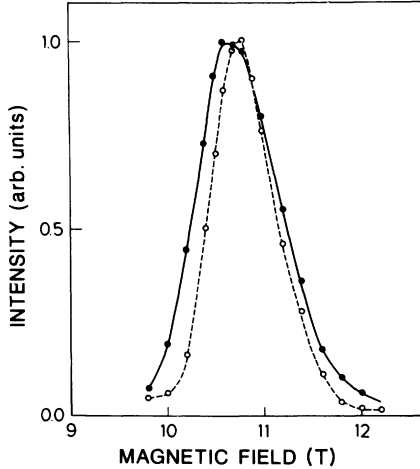


FIG. 3. Resonance profile of the Raman efficiency for scattering by folded acoustic phonons with $\Delta = 9.7 \text{ cm}^{-1}$ (solid line and full circles) and for the background of the secondary emission at the Raman shift $\Delta = 4 \text{ cm}^{-1}$ (dashed line and open circles). The excitation energy is fixed at $\hbar\omega = 1.585 \text{ eV}$, $T = 6 \text{ K}$, sample (98/102, $x = 0.34$, $p = 40$).

Similar oscillations are observed when recording intensity profiles at the Raman shifts of the folded acoustic phonons. Figure 3 shows the resonance profiles for the LA_1 phonon at 9.7 cm^{-1} and for the background emission at 4 cm^{-1} . One can see that incoming and outgoing resonances are unresolved for the LA_1 phonon, as well as for the background. However, the width of the LA_1 resonance is somewhat larger and its maximum is shifted towards smaller magnetic fields, thus reflecting the fact that the separation between incoming and outgoing resonances is larger for the LA_1 phonon scattering at 9.7 cm^{-1} than for the background signal measured at 4 cm^{-1} . It should be noted that the LA_1 phonon profile for the shift of 9.7 cm^{-1} was obtained by measuring the Raman spectra for various magnetic fields and then subtracting the background by hand.

IV. THEORY AND DISCUSSION

A. Geminate recombination

The effect of a magnetic field on the resonant LO-phonon Raman-scattering efficiency has been investigated experimentally¹⁻³ and theoretically⁴⁻⁶ for bulk III-V semiconductors. It was shown that for both Fröhlich and deformation-potential electron-phonon coupling mechanisms, the Raman intensity in a magnetic field has to increase strongly owing to the quasi-one-dimensional character of motion of electrons and holes. In two dimensions the effect should be even stronger, because, in addition to the magnetic-field-induced confinement of electron and hole motion in the xy plane, the quantum-well barriers cause a confinement along the z direction. It is worth noting that the magnetic-field-induced increase of the Raman intensity results from the spatial confinement of electrons and holes by the field.

The specific mechanism of electron-phonon interaction is of no importance for this effect aside from determining its overall strength and, to some extent, the selection rules.

The spectrum of scattered light is determined by two factors: the matrix elements for the electron-photon and electron-phonon interactions and the resonant denominators which appear in the expressions for the scattering efficiency obtained by perturbation theory. The resonant denominators, which are intimately connected to the electronic structure of a given system, specify at which energies and magnetic fields the resonances may appear. The electron-phonon interaction matrix element, on the other hand, plays an important role in the determination of the selection rules for which certain resonances may become observable.

We believe that our results can be explained qualitatively only within a model that takes into account both superlattice and single quantum-well features. The folded acoustic phonons observed in our measurements are a clear manifestation of the superlattice effect. However, it is to be expected that single-quantum-well features are also important. The broadening of the electronic states, as estimated from the resonant profiles, is large enough (1.5 meV for the 100-Å QW, up to 3 meV for the 50-Å QW) to justify the assumption that it originates not only from scattering (homogeneous broadening), but also from some distribution in the widths of the individual QW's (inhomogeneous broadening). Measurements for a 120-Å QW estimated the homogeneous broadening to be just 0.11 meV, much less than the measured inhomogeneous value of 0.55 meV.¹⁴ The inhomogeneous broadening of excitonic resonances by layer thickness fluctuations was also studied by resonant Rayleigh scattering¹⁵ and by temperature-dependent Raman scattering¹⁶ and similar results for the homogeneous linewidths were obtained.

The highly resonant character of the processes we are dealing with makes it plausible that a fraction of the total number of QW's is being selectively probed by choosing specific values of laser frequency and magnetic field. Simple estimations show that even a minute deviation of the QW width from the average value results in energy shifts much larger than the homogeneous broadenings of the observed spectra. For example, a deviation of the width by $\frac{1}{2}$ monolayer for a 100-Å QW results in an energy shift of 3.6 meV for the first size-quantized level. If the homogeneous broadening is smaller than the inhomogeneous one, emission can occur from each single QW without having to conserve k_z along [001]. On the other hand, the perturbation of the overall periodicity is so small that folded acoustic phonons can still be observed.

The background observed in all the measured samples and referred to as *geminate recombination*^{12,17} can be explained by such a single-QW effect. The term *geminate recombination* is intended to express the notion that this secondary emission is due to the recombination of an electron and a hole, which were created together in the same step of photon absorption.¹² We thus consider a model for one-acoustic-phonon Raman scattering in a high magnetic field, assuming deformation-potential interaction of electrons and holes in a single QW with bulklike acous-

tic phonons. The diagram for the amplitude of a process where a phonon is emitted by the electron is shown in the inset of Fig. 4. We make use of the dipole approximation and neglect the penetration of the electron wave function into the barrier. Assuming uncorrelated electron-hole pairs we can write the electron or hole wave function as

$$\Psi_{nNk_y}(\mathbf{r}) = \frac{\exp(ik_y y)}{\sqrt{L_y}} u_n(x - x_{k_y}) \varphi_N(z) v_0(\mathbf{r}), \quad (1)$$

where $L_x L_y$ is the area of a QW. The wave function of a one-dimensional oscillator in the Landau sublevel with the quantum number n is given by

$$u_n(x) = \left(\frac{m\omega_c}{\pi\hbar}\right)^{1/4} \frac{1}{\sqrt{n!}} e^{-\frac{m\omega_c}{2\hbar}x^2} H_n\left(x\sqrt{\frac{2m\omega_c}{\hbar}}\right) \quad (2)$$

with the Hermite polynomials $H_n(x)$. The one-dimensional wave functions for states in the well are

$$\varphi_N(z) = \sqrt{\frac{2}{a}} \cos \frac{\pi N z}{a}, \quad N = 1, 3, 5, \dots, \quad (3)$$

$$\varphi_N(z) = \sqrt{\frac{2}{a}} \sin \frac{\pi N z}{a}, \quad N = 2, 4, 6, \dots \quad (4)$$

with a being the well width and z ranging within the interval $-a/2 \leq z \leq +a/2$; $x_{k_y} = \mp l_B^2 k_y$ for electrons (holes), $l_B = \sqrt{\hbar c/eB}$ being the magnetic length, and $v_0(\mathbf{r})$ the Bloch function. The Hamiltonian for deformation-potential electron-LA-phonon interaction can be written as¹⁸

$$H_{dp} = \sum_{\mathbf{q}} \left(\frac{\hbar a_0^3}{2VM_0\omega_q}\right)^{1/2} iqD e^{i\mathbf{q}\cdot\mathbf{r}} b_{\mathbf{q}} + \text{H. c.}, \quad (5)$$

where D is a deformation-potential constant which is mainly determined by the dependence of the gap on volume and $a_0^3 (M_0)$ is the volume (mass) of the primitive cell. In the dipole approximation it follows directly that q_y is equal to zero (see the diagram in Fig. 4) because of the momentum conservation at the electron-phonon vertex. As for q_x , it can take an arbitrary value in the diagram because there is no conservation for the x component of quasimomentum at the vertex. However, for a given phonon we can always choose the Landau gauge so that its in-plane quasimomentum is along k_y , i.e., $q_x = 0$. The zero value of the transverse component of the phonon wave vector results in the conservation of Landau number n in one-phonon scattering, because

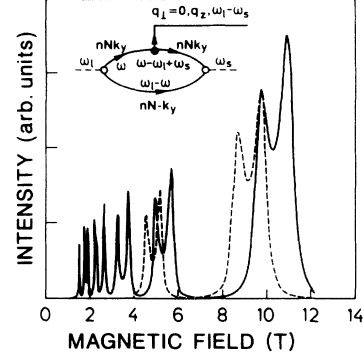


FIG. 4. Calculated dependence of the Raman efficiency vs magnetic field for two polarization configurations $\bar{z}(\sigma^+, \sigma^+)z$ (solid line) and $\bar{z}(\sigma^-, \sigma^-)z$ (dashed line) at a Raman shift of $\Delta = 16 \text{ cm}^{-1}$. For the calculations we used experimentally measured values of the electron and heavy-hole cyclotron energies and their Zeeman splittings. The inset shows the Feynman diagram for the amplitude of one-acoustic-phonon scattering where the phonon with the wave vector ($\mathbf{q}_\perp = 0, q_z$) is emitted by the electron in a transition between two states of a single QW with the same set of quantum numbers (n, N, k_y).

the matrix element for the electron-phonon interaction is nonzero only between states with the same n due to the orthonormality of the functions $u_n(x)$. For one-phonon scattering by acoustic phonons in systems with translational invariance, e.g., bulk semiconductors or a perfectly ordered quantum-well structure, an additional selection rule would require the scattered phonon to take up the difference in crystal momentum q_z between incident and backscattered photons. In bulk material this leads to sharp phonon lines observed in Brillouin scattering, whereas discrete pairs of folded phonons are found for the case of superperiodicity.¹⁹ In the case presented here, the absence of conservation for the component of the quasimomentum q_z along the growth direction is the most important feature, and it explains the continuous emission background observed in the Raman spectra.

We obtain for the matrix element of the electron-phonon interaction

$$\begin{aligned} & \langle \varphi_N(z) | H_{dp} | \varphi_N(z) \rangle \\ &= -i \left(\frac{\hbar a_0^3}{2VM_0\omega_{q_z}}\right)^{1/2} q_z D \frac{\sin \frac{aq_z}{2}}{\frac{aq_z}{2}} \frac{4N^2}{4N^2 - \left(\frac{aq_z}{\pi}\right)^2}. \end{aligned} \quad (6)$$

For the scattering efficiency it follows that

$$\begin{aligned} \frac{1}{V} \frac{d\sigma}{d\omega_s} &= \frac{\omega_s}{\omega_l} \frac{n(\omega_s)}{n(\omega_l)} |\mathbf{e}_l \mathbf{p}_{cv}|^2 |\mathbf{e}_s \mathbf{p}_{cv}|^2 \frac{e^4 a_0^3 D^2}{16\pi^3 c^4 \hbar^3 m_0^4 M_0 a_H^4 a^2} \\ &\times \sum_{q_x} \frac{q_x^2}{\omega_{q_x}} \frac{\sin^2 \frac{aq_x}{2}}{\left(\frac{aq_x}{2}\right)^2} \left| \sum_{nN} \left(\Omega_{nN} + i\frac{\gamma_e + \gamma_h}{2}\right)^{-1} \left(\Omega_{nN} - \omega_l + \omega_s + i\frac{\gamma_e + \gamma_h}{2}\right)^{-1} \frac{4N^2}{4N^2 - \left(\frac{aq_x}{\pi}\right)^2} \right|^2 \\ &\times (n_q + 1) \delta(\omega_l - \omega_s - \omega_q), \end{aligned} \quad (7)$$

where n_q is the Bose-Einstein distribution function for phonons and the parameter

$$\Omega_{nN} = \omega_l - \omega_g - E_N^e/\hbar - E_N^h/\hbar - (n + 1/2)\omega_\mu \quad (8)$$

with the cyclotron frequency $\omega_\mu = eH/\mu c$ is equal to zero in incoming resonance and equal to $\omega_l - \omega_s$ in outgoing resonance. One finds by inspection of Eq. (7) that the scattering efficiency resonates for certain values of the laser frequency and the magnetic field. In a first step, a linear relation is used to model the dispersion of the longitudinal acoustic phonons along the growth direction. From this we calculate a dimensionless quantity proportional to the scattering efficiency. Theoretical results for the Raman spectra obtained by this procedure and scaled to the experimental data are shown by the dashed curve in Fig. 1. In Fig. 4 we show the results of a calculation of the corresponding magneto-oscillations for a Raman shift of 16 cm^{-1} in two polarizations. The profiles were calculated using a detuning energy Ω_{nN} at zero field of 24.4 meV and effective masses determined from the experiment. It should be noticed that according to Eq. (7) phonons with a wide range of q_z contribute to the scattering efficiency. This follows from the absence of conservation of the z component of quasimomentum q_z and leads to a broad spectrum of geminate recombination. The resonant conditions for all phonons in the range of parameters close to the incoming resonance are similar as is confirmed by the data in Fig. 2 (see peaks marked by *). In the case of zero magnetic field, similar calculations also result in resonant behavior of the scattering efficiency. The resonance, however, is of logarithmic character and rather weak compared to the case of a high magnetic field. We also observed the appearance of background recombination and folded phonon Raman scattering with laser excitation in resonance with the ground state of the exciton associated with the next higher ($hh2 - e2$) interband transition. This confirms our conjecture that the spectrum of the scattered light is determined mostly by the matrix element of the electron-phonon interaction.

We find that the assumption of a linear phonon dispersion along the growth direction gives a good description of the geminate recombination background over most of the spectral range. Translational invariance and zone folding, however, are not completely destroyed in the samples which we investigated. The observation of discrete folded phonon doublets and their magneto-resonant behavior in Figs. 1 and 3 is a clear indication of that. In the regions of gaps of the folded phonon dispersion discrepancies from this simplification may be expected to occur. They will be discussed in the next subsection.

Measuring geminate recombination intensity profiles for various excitation wavelengths, fan plots of energy versus resonance magnetic field are obtained. Without paying attention to the specific scattering mechanism, such an experiment can be regarded as a form of magnetophotoluminescence excitation spectroscopy (PLE). In the present case, however, the electronic structure of the system under investigation is tuned by the magnetic field and the detection occurs rather close to the excitation, whereas in conventional PLE the excitation energy is tuned for fixed magnetic fields and the signal is being

detected much farther away, usually at the main peak of the luminescence recombination. Magneto-PLE turned out to be a feasible technique for interband magneto-optical studies in quantum wells and superlattices.²⁰ Using $\mathbf{k} \cdot \mathbf{p}$ theory and the envelope function approach in a basis which describes the mixed structure of the hole subbands and taking excitonic effects into account, a rather detailed agreement with the rich structure observed in the spectra can be achieved.²¹ Preliminary calculations along these lines for the samples investigated here²² show that the oscillations of the emission background reflect interband magneto-optical transitions between valence subband Landau states of heavy mass character and conduction electron states. The resonances in Fig. 2(a) correspond to such transitions with Landau oscillator quantum numbers of the electron states ranging from $n = 1$ to 5.

B. Local phonon modes

Let us now discuss the additional features of the spectrum in Fig. 1. These structures become more pronounced when the sample period is decreased and the Al concentration in the barriers is increased. In Fig. 5 the

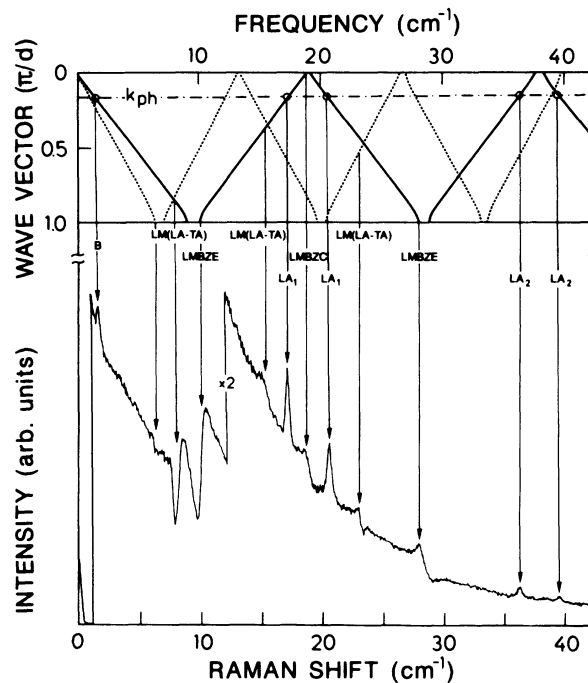


FIG. 5. Raman spectrum of the sample (43/44, $x = 1.00$, $p = 80$) in a magnetic field of $B = 11 \text{ T}$ and $T = 6 \text{ K}$ [$\hbar\omega_{\text{ex}} = 1.727 \text{ eV}$, $\bar{z}(\sigma^-, \sigma^-)z$ configuration] in comparison to the calculated dispersion curves of TA (dotted lines) and LA (solid lines) phonons for this MQW structure. LA_1 and LA_2 are the Raman lines of two doublets of folded acoustic phonons and B is the Brillouin scattering line of LA phonons which one expects to observe in a process with momentum transfer k_{ph} . LMBZE are local modes at zone edge gaps, LMBZC are local modes at zone center gaps, and LM(LA-TA) are local modes at LA-TA crossing gaps.

low-energy part of the Raman spectrum for the (43/44, $x = 1.00$, $p = 80$) sample is compared to the calculated dispersions of folded LA (solid lines) and TA (dotted lines) phonons. The dispersions were calculated according to the elastic model using Eq. (3.5) of Ref. 23. The dominant peaks in the spectrum (LA_1 , LA_2) correspond to Raman scattering by folded LA phonons. These peaks occur as doublets at energies which are determined by the momentum transfer κ_{ph} in the reduced Brillouin zone according to the selection rules for a backscattering geometry in a translationally invariant system. The positions of the structures marked as LMBZC (local mode, Brillouin-zone center), LMBZE (local mode, Brillouin-zone edge), and LM(LA-TA) (local mode at LA/TA crossing), as well as their widths and strengths, depend strongly on the period of the respective MQW structure ($d = d_1 + d_2$) and on the Al content (x) in the barriers. The features can be divided into three groups: (i) structures in the center of two neighboring folded acoustic-phonon doublets (LMBZE); (ii) structures in the center of the two components of the same doublet (LMBZC); (iii) structures which exhibit some periodicity but are not symmetric with respect to the folded phonons [LM(LA-TA)]. Type-(i) structures are found at the positions of the zone-edge gaps for $k = \pi/d$; type-(ii) structures occur at zone-center gaps, i.e., for $k = 0$. For type-(i) and type-(ii) structures it is typical that a minimum is followed by a maximum, and vice versa, for adjacent pairs which correspond to the next zone-edge or zone-center gaps. The energies of type-(iii) features correspond to points in the Brillouin zone where the folded LA and TA branches cross.

We conjecture that these observed features correspond to local vibrational modes originating from fluctuations of the quantum well and barrier thicknesses. In such a case the MQW in the z direction may be considered as a one-dimensional chain with impurities. The dispersion relation for folded phonons in a MQW has the same form as the well-known Kronig-Penney dispersion for electrons in a square-well potential. Therefore the theory of impurity levels in an electronic system²⁴ should be transferable to the present case. It was shown that in such systems any fluctuations of the potential strength or any irregularities in the spacing of layers lead to the appearance of impurity levels inside each forbidden gap of the folded dispersion.²⁴ This is a consequence of the one-dimensional nature of the problem. These impurity levels can be pushed up from the top of the lower band or pulled down from the upper band. The case which is realized in a physical system depends on the sign of the potential fluctuations or on the value of the deviation from regular spacing. In principle this problem can be considered as that of determining gaps in the energy spectrum of a disordered Kronig-Penney model.²⁴ The approach of a disordered Kronig-Penney model should be valid even in the case of very-short-period superlattices. A similar problem has been treated recently in studies of acoustic-phonon transmission resonances in stacked superlattices and double-barrier systems²⁵ as well as in an investigation of vibrational properties of the one-dimensional generalized Fibonacci sequence.²⁶ In both cases the existence

of localized modes inside the folded phonon gaps was suggested theoretically.

Besides the structures discussed above, we observe others [marked LM(LA-TA)] which also repeat periodically in frequency. The positions of these peculiarities coincide with theoretical crossings of the folded LA and TA dispersion curves inside the Brillouin zone. Such gap openings and LA-TA dispersion anticrossings were predicted to occur in Ref. 27. It was shown that for low symmetry growth directions of MQW's such as $[\bar{2}11]$ or $[110]$, the acoustic-phonon modes are not purely longitudinal or transverse. Thus only a quasi-LA and quasi-TA character can be assigned to them. Whenever the dispersions of modes with such mixed character cross, the degeneracy causes a coupling, and an anticrossing occurs. This leads to an opening of gaps inside the Brillouin zone. In our case of a $[001]$ growth direction the LA and TA modes are pure, and an anticrossing should not occur. One can imagine, however, that any defects can cause a deviation from space regularity or changes in the forces at the interfaces. This may lead to a mixing of LA and TA modes and to the opening of a gap with local modes inside. Indications for such anticrossings to occur even along high symmetry axes were also found in Si-Si_{0.5}Ge_{0.5} superlattices grown along the $[111]$ direction.²⁸ Similarly, LA-TA anticrossings have been observed for off-axis propagation in superlattices made of amorphous components.²⁹ We envision that data obtained from Raman scattering by these local modes may yield detailed information on interface quality and disorder.

We want to mention that similar features were observed in Raman spectra from thinner superlattices (14/12, $x = 1.00$) (Ref. 30) under excitation in resonance with some electronic transitions in the absence of a magnetic field. They were then interpreted as antiresonances at the BZ edge with an asymmetry due to the coupling of discrete phonons with a background continuum.³⁰ Resonant measurements of several short-period superlattices grown along different directions ($[001]$, $[111]$, $[012]$) have confirmed the existence of structures related to the BZ edge, even in the absence of magnetic fields.³¹ We conjecture that all these features have the origin discussed above, namely that they are bound vibrational states at the BZ edges. In our experiments these structures appear also for wider quantum wells *provided a strong magnetic field is applied*. In this case the local vibrational modes are induced in Raman scattering by the interplay of interface fluctuations, leading to the appearance of local modes in the phonon spectrum, and the confinement of carriers in a small spatial region due to the well potential, disorder, and the quantizing magnetic field.

V. CONCLUSIONS

We have observed a resonant increase of the Raman-scattering efficiency for folded acoustic phonons and secondary emission (*geminat recombination*) in GaAs-Al _{x} Ga _{$1-x$} As quantum wells in a magnetic field. The occurrence of such emission and its resonant behavior was explained in terms of Raman scattering by effectively bulklike acoustic phonons, which becomes allowed when

the conservation of crystal momentum along the growth direction breaks down. Our experiments present a situation intermediate to ideal superperiodicity and bulk crystal translational invariance. The matrix element of electron-acoustic-phonon deformation-potential interaction was calculated and used to explain the spectra of secondary emission near the excitation line. Additional features in the low-energy Raman spectrum are reported. An interpretation in terms of modes localized inside gaps of the phonon dispersion at the Brillouin zone center and zone edge is given. Another series of modes is found and assigned to local modes inside gaps occurring at folded

LA and TA anticrossings. These gaps, ordinarily forbidden along the [001] growth direction, are suggested to be caused by disorder.

ACKNOWLEDGMENTS

We are grateful to A. J. Shields for a critical reading of the manuscript and for useful comments. We would like to thank A. Fischer and H. P. Schönherr for sample growth, and H. Hirt, M. Siemers, and P. Wurster for first class technical assistance. Two of us (V.F.S. and V.I.B.) acknowledge support from the Max-Planck-Gesellschaft.

*On leave from the A. F. Ioffe Physico-Technical Institute, Russian Academy of Sciences, 194021 St. Petersburg, Russia.

¹G. Ambrazevičius, M. Cardona, and R. Merlin, *Phys. Rev. Lett.* **59**, 700, (1987).

²T. Ruf and M. Cardona, *Phys. Rev. Lett.* **63**, 2288 (1989).

³T. Ruf, R. T. Phillips, C. Trallero-Giner, and M. Cardona, *Phys. Rev. B* **41**, 3039 (1990).

⁴R. Enderlein and F. Bechstedt, *Phys. Status Solidi B* **80**, 225 (1977).

⁵C. Trallero-Giner, T. Ruf, and M. Cardona, *Phys. Rev. B* **41**, 3028 (1990).

⁶V. I. Belitsky, A. V. Goltsev, I. G. Lang, and S. T. Pavlov, *Zh. Eksp. Teor. Fiz.* **86**, 272 (1984) [*Sov. Phys. JETP* **59**, 155 (1984)].

⁷D. Gammon, R. Merlin, and H. Morkoç, *Phys. Rev. B* **35**, 2552 (1987).

⁸D. Gammon, L. Shi, R. Merlin, G. Ambrazevičius, and K. Ploog, *Superlatt. Microstruct.* **4**, 405 (1988).

⁹F. Calle, J. M. Calleja, F. Meseguer, C. Tejedor, L. Viña, C. López, and K. Ploog, *Phys. Rev. B* **44**, 1113 (1991).

¹⁰A. Cros, A. Cantarero, C. Trallero-Giner, and M. Cardona, *Phys. Rev. B* **45**, 6106 (1992).

¹¹A. Cros, A. Cantarero, C. Trallero-Giner, and M. Cardona, *Phys. Rev. B* **XX**, XXXX (1992).

¹²P. S. Kop'ev, D. N. Mirlin, V. F. Sapega, and A. A. Sirenko, *Pis'ma Zh. Eksp. Teor. Fiz.* **51**, 624 (1990) [*JETP Lett.* **51**, 708 (1990)].

¹³V. F. Sapega, T. Ruf, M. Cardona, K. Ploog, E. L. Ivchenko, and D. N. Mirlin (unpublished).

¹⁴J. Kuhl, A. Honold, L. Shultheis, and C. W. Tu, in *Festkörperprobleme*, Vol. 29 of *Advances in Solid State Physics* (Vieweg, Braunschweig, 1989), p. 157.

¹⁵J. Hegarty, M. D. Sturge, C. Weisbuch, A. C. Gossard, and W. Wiegmann, *Phys. Rev. Lett.* **49**, 930 (1982).

¹⁶J. E. Zucker, A. Pinczuk, D. S. Chemla, and A. C. Gossard, *Phys. Rev. B* **35**, 2892 (1987).

¹⁷D. N. Mirlin, P. S. Kop'ev, I. I. Reshina, V. F. Sapega, and A. A. Sirenko, in *Proceedings of the 20th International Conference on the Physics of Semiconductors*, edited by E. M. Anastassakis and J. D. Joannopoulos (World Scientific, Singapore, 1990), p. 1037.

¹⁸A. Pinczuk and E. Burstein, in *Light Scattering in Solids I*, Vol. 8 of *Topics in Applied Physics*, edited by M. Cardona (Springer, Heidelberg, 1983), p. 23.

¹⁹M. V. Klein, *IEEE J. Quantum Electron.* **22**, 1760 (1986).

²⁰G. Belle, J. C. Maan, and G. Weimann, *Solid State Commun.* **56**, 65 (1985).

²¹F. Ancilotto, A. Fasolino, and J. C. Maan, *Phys. Rev. B* **38**, 1788 (1988).

²²A. Cros and A. Cantarero (private communication).

²³B. Jusserand and M. Cardona, in *Light Scattering in Solids V*, Vol. 66 of *Topics in Applied Physics*, edited by M. Cardona and G. Güntherodt (Springer, Heidelberg, 1989), p. 61.

²⁴J. Hori, in *Spectral Properties of Disordered Chains and Lattices*, Vol. 16 of *International Series of Monographs in Natural Philosophy*, general editor: D. ter Haar (Pergamon, Oxford, 1968).

²⁵S. Mizuno and S. Tamura, *Phys. Rev. B* **45**, 734 (1992); **45**, 13423 (1992).

²⁶W. Xu, *Solid State Commun.* **82**, 645 (1992).

²⁷F. Calle, M. Cardona, E. Richter, and D. Strauch, *Solid State Commun.* **72**, 1153 (1989).

²⁸A. B. Talochkin, V. A. Markov, I. G. Neizvestnyĭ, O. P. Pchelyakov, M. P. Sinyukov, and S. I. Stenin, *Pis'ma Zh. Eksp. Teor. Fiz.* **50**, 21 (1989) [*JETP Lett.* **50**, 24 (1989)].

²⁹P. V. Santos, L. Ley, J. Mebert, and O. Koblinger, *Phys. Rev. B* **36**, 4858 (1987).

³⁰C. Colvard, T. A. Gant, M. V. Klein, R. Merlin, R. Fischer, H. Morkoç, and A. C. Gossard, *Phys. Rev. B* **31**, 2080 (1985).

³¹D. J. Mowbray (private communication).